

# ANISOTROPY IN THE COSMIC MICROWAVE BACKGROUND AT DEGREE ANGULAR SCALES: PYTHON V RESULTS

K. COBLE<sup>1</sup>, M. DRAGOVAN<sup>1</sup>, J. KOVAC<sup>1</sup>, N. W. HALVERSON<sup>1,8</sup>, W. L. HOLZAPFEL<sup>1</sup>, L. KNOX<sup>1</sup>,  
S. DODELSON<sup>1,2</sup>, K. GANGA<sup>3,8</sup>, D. ALVAREZ<sup>4</sup>, J. B. PETERSON<sup>4</sup>, G. GRIFFIN<sup>4</sup>, M. NEWCOMB<sup>4</sup>,  
K. MILLER<sup>5</sup>, S. R. PLATT<sup>6</sup>, G. NOVAK<sup>7</sup>

*Draft version March 23, 2019*

## ABSTRACT

Observations of the microwave sky using the Python telescope in its fifth season of operation at the Amundsen-Scott South Pole Station in Antarctica are presented. The system consists of a 0.75 m off-axis telescope instrumented with a HEMT amplifier-based radiometer having continuum sensitivity from 37-45 GHz in two frequency bands. With a  $0.91^\circ \times 1.02^\circ$  beam the instrument fully sampled 598 deg<sup>2</sup> of sky, including fields measured during the previous four seasons of Python observations. Interpreting the observed fluctuations as anisotropy in the cosmic microwave background, we place constraints on the angular power spectrum of fluctuations in eight multipole bands up to  $l \sim 260$ . The observed spectrum is consistent with both the COBE experiment and previous Python results. There is no significant contamination from known foregrounds. The results show a discernible rise in the angular power spectrum from large ( $l \sim 40$ ) to small ( $l \sim 200$ ) angular scales. The shape of the observed power spectrum is not a simple linear rise but has a sharply increasing slope starting at  $l \sim 150$ .

*Subject headings:* cosmic microwave background - cosmology: observations

## 1. INTRODUCTION

Measurement of anisotropy in the Cosmic Microwave Background (CMB) directly probes conditions of the early universe. Observations of the angular power spectrum of CMB temperature fluctuations can be used to test theories of structure formation and constrain cosmological parameters. Results from the COBE satellite (Smoot et al. 1992) tightly constrain the angular power spectrum at the largest angular scales. Several experiments have measured the angular power spectrum at degree angular scales (e.g., Gaier et al. 1992, Schuster et al. 1993, Gundersen et al. 1995, Lim et al. 1996, Platt et al. 1997, Cheng et al. 1997, Netterfield et al. 1997, Devlin et al. 1998, Herbig et al. 1998). Collectively the data show a rise in power towards smaller angular scales; individually no experiment covers a wide range of angular scales from COBE scales to degree scales, and most cover only small regions of the sky. The dataset from the fifth Python observing season (hereafter PyV) has sufficient sky coverage to probe the smallest scales to which COBE was sensitive, while having a small enough beam to detect the rise in angular power at degree angular scales.

In its first four seasons the Python experiment detected significant anisotropy in the CMB (Dragovan et al. 1994 (PyI), Ruhl et al. 1995 (PyII), Platt et al. 1997 (PyIII), Kovac et al. 1999 (PyIV)). Observations from the first three seasons were made at 90 GHz with a bolometer sys-

tem and a 4-point chop scan strategy, yielding CMB detections at angular scales of  $l \sim 90$  and  $l \sim 170$ . During the PyIV season measurements were made using the same scan strategy with a HEMT amplifier-based radiometer, confirming PyI-III detections in a 37-45 GHz frequency band.

Observations were made from November 1996 through February 1997 in the fifth Python observing season. In order to increase the range of observed angular scales, a smoothly scanning sampling scheme was implemented. As a result, PyV is sensitive to the CMB angular power spectrum from  $l \sim 40$  to  $l \sim 260$ .

## 2. INSTRUMENT

The PyV measurements were made using the same receiver as the PyIV system as described in Alvarez (1996) and Kovac et al. (1999). The receiver consists of two focal-plane feeds, each with a single 37-45 GHz HEMT amplifier. A diplexer splits each signal at  $\sim 41$  GHz before detection, giving four data channels. The analysis reported here eventually combines signals from all four channels, resulting in a thermal radiation centroid  $\nu_c = 40.3$  GHz and effective passband  $\Delta\nu = 6.5$  GHz for the PyV dataset.

The receiver is mounted on a 0.75 m diameter off-axis parabolic telescope (Dragovan et al. 1994), which is surrounded by a large ground shield to block stray radiation from the ground and Sun. The beams corresponding to the

<sup>1</sup>Enrico Fermi Institute, University of Chicago

<sup>2</sup>Fermilab

<sup>3</sup>IPAC

<sup>4</sup>Carnegie-Mellon University

<sup>5</sup>University of Colorado

<sup>6</sup>University of Arizona

<sup>7</sup>Northwestern University

<sup>8</sup>California Institute of Technology

two feeds observe the same elevation and are separated by  $2.80^\circ$  on the sky. These beams are scanned horizontally across the sky by a large rotating vertical flat mirror, the chopper, at 5.1 Hz. The new scan strategy motivated two changes from the instrument configuration described in Kovac et al. (1999): the frequency response of the data system was extended by switching to 100 Hz-rolloff antialiasing Bessel filters, and the data recording rate was correspondingly increased, to 652.8 samples/sec for each channel.

### 3. CALIBRATION

As in previous Python seasons, the primary DC calibration of the detectors was derived using liquid nitrogen, liquid oxygen, and ambient temperature thermal loads (Dragovan et al. 1994, Ruhl et al. 1995). Load calibrations were performed approximately once per day, and gains were found to be consistent over the entire season to within  $\pm 2\%$ , with no discernible trends. Gain compression, which was a source of systematic uncertainty in the calibration of PyI-PyIII, is measured to be negligible for the Python HEMT receiver. Systematic uncertainty in the DC load calibration is estimated to be  $\pm 10\%$ .

Several efficiencies must be estimated to relate the load calibrations to celestial response in the main beam, which account for power losses in the atmosphere, in the sidelobes, and in the telescope, and they are calculated using data from skydips and from various beam measurements. The resulting systematic calibration uncertainty of  $+10\%$  to  $-4\%$  is asymmetric, due to the fact that the individual losses are small positive numbers and hence the errors in their estimation follow skewed distributions (Kovac et al. 1999).

The dynamic response of the system was calculated from laboratory measurements of the transfer functions for the AC coupling and antialiasing filters in the data system, and confirmed on the telescope by comparison of observations made of the moon using normal and slow chopper speeds. The response speed of the detectors is not a concern for this calibration or for its uncertainty. An appropriate response correction factor is applied to each modulation of the data. The uncertainty on these factors is small, and is dominated by a  $\pm 5\%$  systematic uncertainty on their common normalization.

The overall uncertainty in the calibration of this dataset is estimated to be  $+15\%$  to  $-12\%$ . Antenna temperature has been converted to units of  $\delta T_{\text{CMB}}$  throughout.

### 4. OBSERVATIONS

Two regions of sky were observed: the PyV main field, a  $7.5^\circ \times 67.7^\circ$  region of sky centered at  $\alpha = 23.18^h$ ,  $\delta = -48.58^\circ$  (J2000) which includes fields measured during the previous four seasons of Python observations and a  $3.0^\circ \times 30.0^\circ$  region of sky centered at  $\alpha = 3.00^h$ ,  $\delta = -62.01^\circ$  (J2000), which encompasses the region observed with the ACME telescope (Gundersen et al. 1995). The total sky coverage for the PyV regions is  $598 \text{ deg}^2$ , greater sky coverage than previous degree-scale CMB experiments. The combined absolute and relative pointing uncertainty is estimated to be  $0.15^\circ$ , as determined by measurements of the moon and the Carinae nebula ( $\alpha = 10.73^h$ ,  $\delta = -59.65^\circ$ ). The PyV beam is well approximated by an asymmetric Gaussian of FWHM  $0.91_{-0.01}^{+0.03} \times 1.02_{-0.01}^{+0.03}$  degrees ( $az \times el$ ).

The beam is determined from scans of the Carinae nebula and the Moon. Both PyV regions are fully sampled with a grid spacing of  $0.92^\circ$  in elevation and  $2.5^\circ$  in right ascension, corresponding to a distance of  $1.6^\circ$  on the sky at a declination of  $-50^\circ$ . The telescope is positioned on one of the fields and the chopper smoothly scans the beams in azimuth in a nearly triangular wave pattern. The chopper throw is  $17^\circ$  in azimuth, corresponding to  $11^\circ$  on the sky at a declination of  $-50^\circ$ . A total of 345 fields are observed in 27 sets of 5–17 fields. There are 128 data samples for each detector channel in a complete chopper cycle, and 164 chopper cycles of data are taken of a given field before the telescope is positioned on the next field in the set. One data file consists of 164 chopper cycles for each field in the set. Approximately 10 hours of good data (100 files) are taken of a set of fields before the telescope moves on to the next set of fields.

### 5. DATA REDUCTION

After cutting 45% of the data for weather and tracking errors, 389 hours of data remained for use in the CMB analysis. The data are modulated using

$$M_m(\theta) = \cos(m\pi\theta/\theta_c) \times \begin{cases} 1 & m = 1 \\ H(\theta) & m = 2 \dots 9 \end{cases} \quad (1)$$

where  $m$  is the modulation number,  $\theta$  is the chopper angle,  $\theta_c$  is the extent of the chopper throw and  $H(\theta) = 0.5(1 - \cos(2\pi\theta/\theta_c))$  is a Hann window (Fig. 1). The  $m = 2 \dots 9$  modulations are apodized with the Hann window in order to reduce the ringing of the window functions in  $l$ -space. Data taken during the right- and left-going portions of the chopper cycle are modulated separately, to allow for cross-checks of the data. Sine modulations are not used in the analysis because they are anti-symmetric and are thus sensitive to gradients.

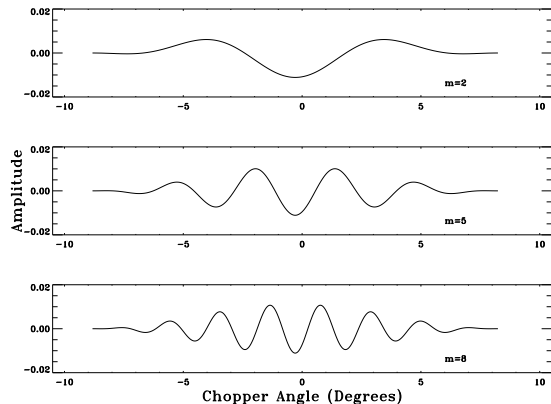


FIG. 1.— The data are modulated with cosines which have been apodized by a Hann window. Three of the modulations are shown.

Data in a given file, field, channel, and modulation are co-added over all chopper cycles. A chopper synchronous offset, due to differential spillover past the chopper, is removed from each data file by subtracting the average of all of the fields in a file. This is not just a DC offset; there is an offset removed for each modulation (or equivalently, for each sample of the chopper waveform) and channel. This subtraction must be accounted for by adding a term to the covariance matrix (see section 6). When the data are binned in azimuth, a periodic signal due to the 12 panels of the ground shield is evident, especially on larger angu-

lar scales. The signal of period  $30^\circ$  is fit for an amplitude and is subtracted. Removal of the ground shield offset has less than 4% effect on the final angular power spectrum (section 6) in all modulations.

After the data have been modulated and offsets removed, the right and left-going data, which have been properly phased, are co-added, as are channels which observe the same points on the sky. Since the two feeds observe different points on the sky they cannot be co-added; the theoretical and noise covariances between them are included in the likelihood analysis of the angular power spectrum.

The South Pole Station power nominally operates at a frequency of 60 Hz, so there is possible contamination at 60 Hz and its harmonics. However, the phase is randomized every cycle, and all cycles in a file are averaged, so the 60 Hz source is washed out. To test this, we created a 60 Hz signal for one stare of data, modulated it, averaged over 164 cycles and found that the 60 Hz signal is negligible. Since the chopper runs at 5.1 Hz, our modulations are not sensitive to 60 Hz.

Our noise model assumes the covariance between fields taken with different sets of files is negligible because of the chopper offset removal and because of the long time (at least 10 hours) between measurements. An analysis comparing the noise covariance estimated from data which had not yet been co-added over all cycles and the noise covariance estimated from data which had been co-added over all cycles indicates that PyV noise is dominated by detector noise. However, the long term drifts due to the atmosphere, which add to the variance as well as induce small correlations between fields taken with the same set of files, are important, especially for power spectrum estimation (section 6). The noise covariance between fields taken with the same set of files is first estimated by taking the usual covariance on the co-added data, but because there were typically only 100 files taken for each field, the sample variance on the noise estimate is  $\sim (100)^{1/2}$ , or 10%, which will severely bias estimates of band power. To obtain a better estimate of the noise, we averaged the variances for each set of files and then scaled the off-diagonal elements of the covariance to the average variance in a given set based on a model derived from the entire PyV data set.

Several self-consistency checks were performed on the data set, using our best estimate of the noise covariance. The  $\chi^2 = \mathbf{d}^t C^{-1} \mathbf{d}$ , where  $\mathbf{d}$  is the data vector and  $C = C^T + C^N + C^C$  is the total covariance (see section 6), is consistent with its expected value (the number of degrees of freedom) in all modulations. The value of the probability enhancement factor,  $\beta$ , (Knox et al. 1998) between data from the two feeds falls within the expected range for all modulations. Finally, the data set was transformed into the signal-to-noise eigenmode basis. In that basis,  $C^{-1} \mathbf{d}$  should be Gaussian distributed with  $\sigma = 1$  and a total area equal to the number of degrees of freedom. Histograms of  $C^{-1} \mathbf{d}$  are consistent with such a Gaussian distribution for all of the modulations. We performed these same tests using the preliminary noise covariance, which suffers from sample variance, and found that the consistency tests failed. The tests indicate that the data set used is self consistent and that our best estimate of the noise covariance is indeed a good model for the noise.

## 6. DATA ANALYSIS AND RESULTS

CMB angular power is usually expressed in terms of angular multipoles,  $C_l$ . A flat power spectrum is one for which  $\mathcal{C} \equiv (l(l+1)C_l/2\pi)$  is constant. For each of the eight modulations, we compute the likelihood ( $\mathcal{L}$ ) as a function of  $\mathcal{C}$ . The theoretical covariance matrix,  $C^T$ , needed to compute  $\mathcal{L}$  depends on the amplitude of  $\mathcal{C}$  and the experimental window functions. The window functions are a measure of experimental sensitivity as a function of angular scale  $l$  (Fig. 2). They are generated from the experimental beam map, modulations, and observing strategy and are given by

$$W_{lij} = (1/2\pi) \int d\phi e^{-i\mathbf{k}\cdot(\mathbf{x}_i - \mathbf{x}_j)} \tilde{B}(\mathbf{k}) \tilde{B}^*(\mathbf{k}) \quad (2)$$

where  $\tilde{B}(\mathbf{k})$  is the Fourier transform of the beam map for the given modulation,  $\mathbf{x}_i$  the position of field  $i$ , and  $\mathbf{k} = l(\cos \phi, \sin \phi)$ . These functions are computed for all pairs of fields and channels.

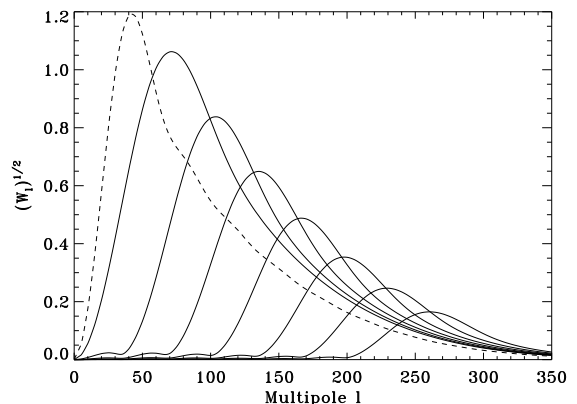


FIG. 2.— Diagonal window functions. The unapodized cosine modulation is plotted with a dashed line and the apodized cosine modulations are plotted with solid lines.

The subtraction of the chopper synchronous offset can be accounted for as an additional term in the covariance matrix (e.g., (Bond et al. 1998)) and in this case is given by:

$$C^C = (K/N_{\text{files}}) \left( \sum_s M_s M_s \right) \quad (3)$$

for fields taken with the same set of files and zero for fields not taken with the same set of files.  $M_s$  is the given modulation as a function of chopper sample  $s$  (Eq. 1), and  $N_{\text{files}}$  is the number of files which observed the fields. Taking  $K$  to be large ensures that we have no sensitivity to modes of the data that could have come from the chopper.

The CMB power spectrum is shown in Fig. 3 and is given in Table 1. The band powers shown in Fig. 3 are calculated for each modulation separately. This neglects the correlations between modulations. Work is in progress to fit the amplitudes in a series of bands to all of the modulations simultaneously. The calibration uncertainty allows all band powers to shift by the same amount (i.e. the calibration errors are correlated). Given the uncertainty in the beam size of approximately  $0.015^\circ$ , the band power for a given modulation can move roughly by a factor of  $\exp(\pm l(0.425)(0.015)(\pi/180))$ , only a 3% effect at  $l = 200$ . Flat band powers calculated from the subset of PyV data

in the PyIII region of sky are consistent with the PyIII flat band powers to within the uncertainties. Given the  $+15\%$  calibration uncertainty and the  $3\mu\text{K}$  statistical uncertainty, the lowest  $l$  PyV modulation agrees with the the smallest scale COBE measurements.

Table 1

Results of likelihood analysis. Band powers are in  $\mu\text{K}$ .

mode	$l_e$	$(l(l+1)C_l/2\pi)^{1/2}$
1	$50^{+44}_{-29}$	$23^{+3}_{-3}$
2	$74^{+39}_{-41}$	$26^{+4}_{-4}$
3	$108^{+49}_{-41}$	$31^{+4}_{-4}$
4	$140^{+45}_{-41}$	$28^{+11}_{-13}$
5	$172^{+43}_{-40}$	$54^{+10}_{-10}$
6	$203^{+41}_{-39}$	$98^{+14}_{-14}$
7	$233^{+40}_{-38}$	$90^{+53}_{-90}$
8	$264^{+39}_{-37}$	$0^{+92}_{-0}$

## 7. FOREGROUNDS

The PyV data are cross-correlated with several foreground templates in order to set limits on possible foreground contamination. The templates used are the Schlegel et al. (1998) 100 micron dust map, which is based on IRAS and DIRBE maps, the Haslam et al. (1974) 408 MHz survey (synchrotron), and the PMN survey (point sources). Each foreground template map is smoothed to PyV resolution, pixelized and modulated according to the PyV observation scheme.

Two templates are created for the PMN survey. We call one PMN, which is converted to  $\delta T_{\text{CMB}}$  using the spectral indices given in the survey. The other we call PMN0, which is converted to a flux at 40 GHz assuming a flat spectrum extrapolated from the flux measurement at 4.85 GHz. The assumption of a flat spectrum is conservative in that it is likely to over-estimate the flux at 40 GHz. Neither case is correct, since spectral indices have not been measured for all of the sources, in which case a flat spectrum is assumed, but we do know that some of them are not flat, so a flat spectrum will be inappropriate. The two cases cover a reasonable range of possibilities.

For each modulation and foreground template, a correlation coefficient and uncertainty are calculated following de Oliveira-Costa et al. (1997). A weighted mean and uncertainty over all of the modulations for each foreground are given in Table 2. In all cases there is no clear detection of foregrounds. The RMS of each modulation of each foreground was calculated and then multiplied by the corresponding  $1\sigma$  error bar in Table 2 in order to estimate an upper limit on the foreground contribution to CMB band power. The limits on contributions from foregrounds are

given in Table 3 and are at least  $\sim 10\times$  smaller than the measured CMB bandpowers.

Table 2

Correlation coefficients and uncertainties for weighted means.			
Dust	Haslam	PMN	PMN0
$\mu\text{K}(MJy/sr)^{-1}$	$\mu\text{K}/\text{K}$	$\mu\text{K}/\mu\text{K}$	$\mu\text{K}(MJy/sr)^{-1}$
$-3 \pm 18$	$-2.0 \pm 2.6$	$0.012 \pm 0.024$	$195 \pm 385$

Table 3

Limits on foreground contribution. All units are  $\mu\text{K}$ .

Mode	Dust	Haslam	PMN	PMN0
1	1.0	0.5	0.3	0.3
2	1.0	0.6	0.6	0.6
3	1.1	0.8	1.0	1.0
4	1.1	1.0	1.1	1.1
5	1.9	2.7	2.7	2.7
6	2.7	6.7	5.4	5.4
7	2.0	6.9	5.9	5.9
8	1.6	8.2	6.6	6.6

If the diffuse morphology of the sky is not constant as a function of wavelength, then these templates do not reveal all of the foreground contamination and more could be hidden in the PyV data. A combined analysis of PyIII at 90 GHz and PyV at 40 GHz would constrain the foreground contamination further. When the data themselves are analyzed as a whole, rather than separately for each modulation, the foreground analysis will also be done on the data set as a whole. This will take into account the cross-modulation correlations in the data.

## 8. CONCLUSIONS

The PyV experiment fully samples  $598 \text{ deg}^2$  of the microwave sky and constrains the CMB angular power spectrum in the angular scale range  $40 \lesssim l \lesssim 260$ . The measurements pass internal consistency checks, show little contamination from foreground radiation, and are consistent with previous Python and COBE results. The observed angular power increases from larger to smaller angular scales, with a sharply increasing slope starting at  $l \sim 150$ .

We would like to thank Bharat Ratra for helpful conversations and for generously aiding us in checking our window functions. This work was supported by the James S. McDonnell Foundation, PYI grant NSF AST 90-57089, and the NSF under a cooperative agreement with the Center for Astrophysical Research in Antarctica (CARA), grant NSF OPP 89-20223. CARA is an NSF Science and Technology Center. The work of SD was supported by NASA Grant NAG 5-7092 (in addition to the DOE). KG acknowledges support from NASA ADP grant NASA-1260. KC is supported by NASA NGT 5-19.

## REFERENCES

- Alvarez, D. 1996, Ph.d. thesis, Princeton Univ.  
 Bond, J. R., Jaffe, A., and Knox, L. 1998, Phys. Rev. D, 57, 2117  
 Cheng, E. S., et al. 1997, ApJ, 488, L59  
 de Oliveira-Costa, A., et al. 1997, ApJ, 482, 17  
 Devlin, M., et al. 1998, ApJ, 509, L69  
 Dragovan, M., et al. 1994 ApJ, 427, L67 (PyI)  
 Gaier, T. et al. 1992, ApJ, 398, L1  
 Gundersen, J. O., et al. 1995, ApJ, 443, L57  
 Haslam, C.G.T. et al. 1974, A&AS, 13, 369  
 Herbig, T., et al. 1998, ApJ, 509, L73  
 Kovac, J., et al. 1999, in preparation (PyIV)  
 Knox, L., et al. 1998, Phys. Rev. D, 58, 083004  
 Lim, M. A., et al. 1996, ApJ, 469, L69  
 Netterfield, C. B., et al. 1997, ApJ, 474, 47  
 Platt, S. R., et al. 1997, ApJ, 475, L1 (PyIII)  
 Ruhl, J. E., et al. 1995, ApJ, 453, L1 (PyII)  
 Schuster, J. et al. 1993, ApJ, 412, L47  
 Schlegel, D. J., Finkbeiner, D. P. and Davis, M. 1998, ApJ, 500, 525  
 Smoot, G. F., et al. 1992, ApJ, 396, L1

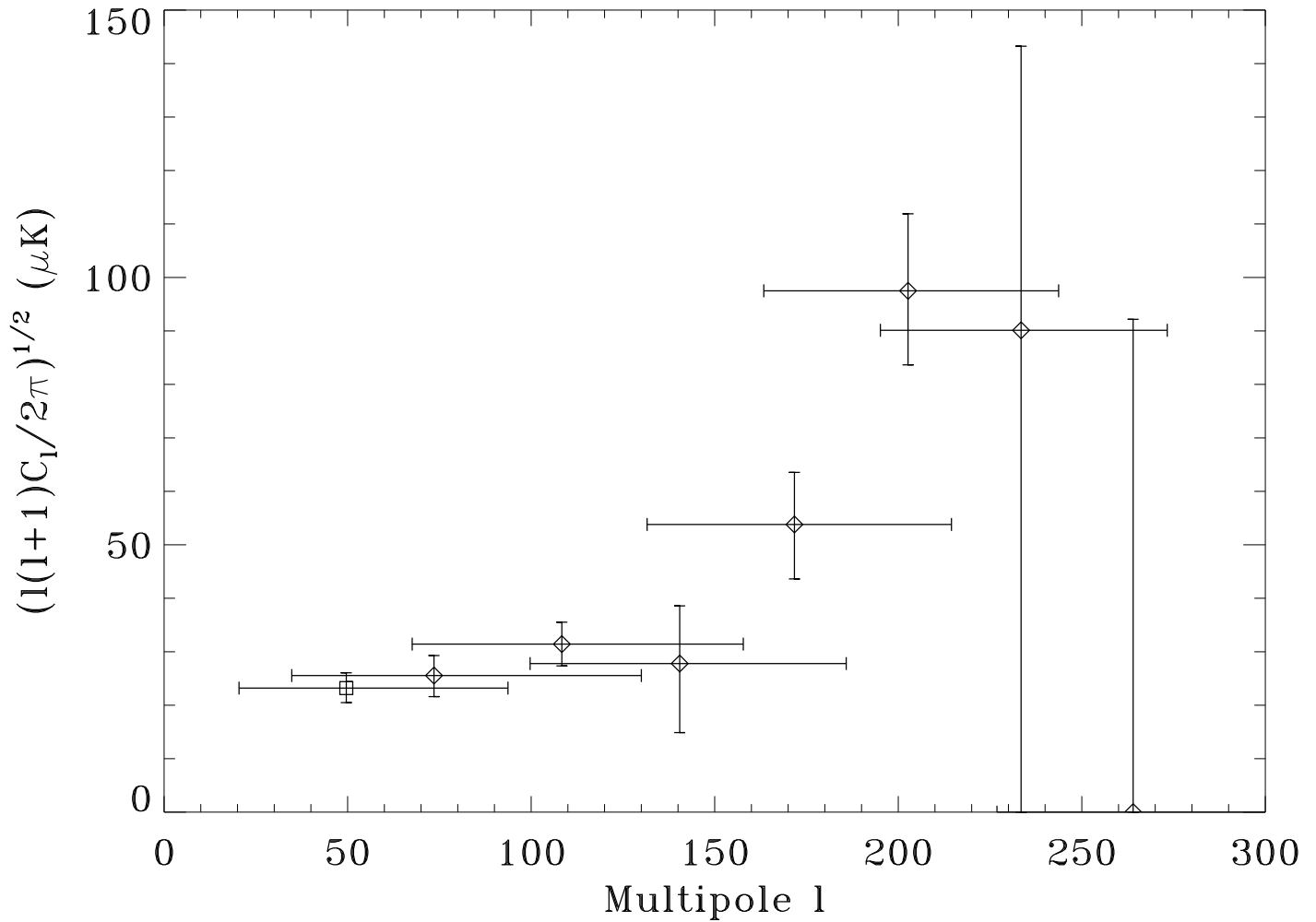


FIG. 3.— Flat band power,  $(l(l+1)C_l/2\pi)^{1/2}$ , vs. multipole  $l$  for all of the modulations. The detections have  $1\sigma$  error bars and the upper limit has  $2\sigma$  error bars. The unapodized cosine modulation is plotted with an open square and the apodized cosine modulations are plotted with diamonds. The error bars include statistical uncertainties only and do not include uncertainties in the calibration or beam size. The  $l$  range of each modulation is determined by the half-maximum points of  $(W_l)^{1/2}$ . Low  $l$  values correspond to large angular scales and high  $l$  values correspond to small angular scales. CMB power is clearly rising from low to high  $l$  up to the sensitivity cutoff of PyV.